# Evidence for a phosphorus-related interfacial defect complex at a GaP/GaNP heterojunction

D. Dagnelund,[1] I. P. Vorona,[2] L. S. Vlasenko,[3] X. J. Wang,[1] A. Utsumi,[4] Y. Furukawa,[4] A. Wakahara,[4] H. Yonezu,[4] I. A. Buyanova,[1] and W. M. Chen[1]

[1]*Department of Physics, Chemistry and Biology, Linköping University, S-581 83 Linköping, Sweden*

[2]*Institute of Semiconductor Physics, National Academy of Sciences of Ukraine, Kiev 03028, Ukraine*

[3]*A. F. Ioffe Physico-Technical Institute, St. Petersburg 194201, Russia*

[4]*Department of Electrical and Electronic Engineering, Toyohashi University of Technology, Toyohashi, Aichi 441-8580, Japan*

(Received 3 February 2010; revised manuscript received 9 March 2010; published 31 March 2010)

Optically detected magnetic resonance (ODMR) studies of molecular beam epitaxial GaNP/GaP structures reveal presence of a P-related complex defect, evident from its resolved hyperfine interaction between an unpaired electronic spin ($S=1/2$) and a nuclear spin ($I=\frac{1}{2}$) of a $^{31}$P atom. The principal axis of the defect is concluded to be along a ⟨111⟩ crystallographic direction from angular dependence of the ODMR spectrum, restricting the P atom (either a $P_{Ga}$ antisite or a $P_i$ interstitial) and its partner in the complex defect to be oriented along this direction. The principal values of the electronic $g$ tensor and hyperfine interaction tensor are determined as: $g_{\perp}=2.013$, $g_{\parallel}=2.002$, and $A_{\perp}=130\times10^{-4}$ cm$^{-1}$, $A_{\parallel}=330\times10^{-4}$ cm$^{-1}$, respectively. The interface nature of the defect is clearly manifested by the absence of the ODMR lines originating from two out of four equivalent ⟨111⟩ orientations. Defect formation is shown to be facilitated by nitrogen ion bombardment under nonequilibrium growth conditions and the defect is thermally stable upon post-growth thermal annealing.

DOI: 10.1103/PhysRevB.81.115334 PACS number(s): 76.70.Hb, 71.55.Eq, 68.35.Dv, 61.72.J−

## I. INTRODUCTION

Heterojunctions between two dissimilar solids and associated interfaces are of high scientific interest in physics, chemistry, and material science of solid states. They also play an important role in many modern device applications, as heterojunctions and heterointerfaces are either among key components defining functionalities of devices or being inevitably encountered. For example, achieving high quality $Si/SiO_2$ interfaces by controlling interfacial defects (dominated by silicon dangling bonds) have been a decisive factor in the success of silicon in integrated circuit technology that is based on metal-oxide-semiconductor field-effect transistors. Heterojunctions between two different semiconductors have been the key to the success of, e.g., high electron mobility transistors (HEMT) used for radars and millimeter wave communications, heterojunction bipolar transistors (HBT) used in power amplifiers, and modern nanodevice and quantum devices such as quantum well or quantum dot lasers for CD/DVD and fiber-optic communications. Here, the performance of the devices is largely controlled by structural quality of the interfaces and interfacial defects. In the case of $Si/SiO_2$ interfaces the dominant defects have been positively identified[1–3] as being Si dangling bonds when the silicon crystal is jointed with the oxides of a different crystal structure. Very little is known about origin of interfacial point defects at *semiconductor* heterojunctions, on the other hand, despite of the fact that they can severely restrict carrier mobility, minority carrier lifetime and radiative efficiency[4,5] that are the key parameters determining the performance of, e.g., HEMT, HBT, and light-emitting devices. In this paper we report on the first identification of a point defect situated at an interface between two semiconductors: GaNP and GaP. We shall show that the defect is a complex involving a P atom in its core, partnered by an impurity/defect oriented along a ⟨111⟩ direction. The character of electron wave function and formation of the defect during molecular beam epitaxy (MBE) growth will also be discussed.

The studied GaNP alloys belong to an interesting class of dilute nitrides that have attracted great attention in recent years owing to their fascinating physical properties, which are drastically different from other conventional semiconductor alloys and arise from the large mismatch in atomic size and electronegativity between anion atoms.[6,7] They also hold great potential in novel optoelectronic and electronic applications. For example, GaNP can be grown lattice matched to Si, opening new possibilities to combine high optical efficiency of the III-V compound semiconductors with the mainstream microelectronics based on silicon, yielding, e.g., novel optoelectronic integrated circuits based on GaNP/Si.[8,9] GaInNP alloys lattice matched to GaAs are expected to greatly improve the performance of GaInNP/GaAs HBTs.[10] For full exploration of the dilute nitrides in device applications, a better understanding and control of defects located at interfaces involving Ga(In)NP are required.

## II. SAMPLES AND EXPERIMENTAL METHOD

Two GaNP/GaP structures were studied in this work, hereafter referred to as samples L021 and L022. They were both grown at 590 °C on (001) GaP substrates by solid-source MBE. The growth started with a 100-nm thick GaP buffer layer, followed by a 100-nm GaNP, and was finally capped by a 20-nm thick GaP layer. Incorporation of N was accomplished by using a RF-plasma cell to supply N radicals. N composition of 0.5% in the GaNP alloy was determined by the photon energy of the main photoluminescence (PL) peak near the band edge at 5K, from a comparison with its known dependence on N content reported in earlier studies.[11] To study effect of N-ion bombardment on formation of the studied defect, an ion collector was employed during the growth of the sample L021 but not L022. The

 

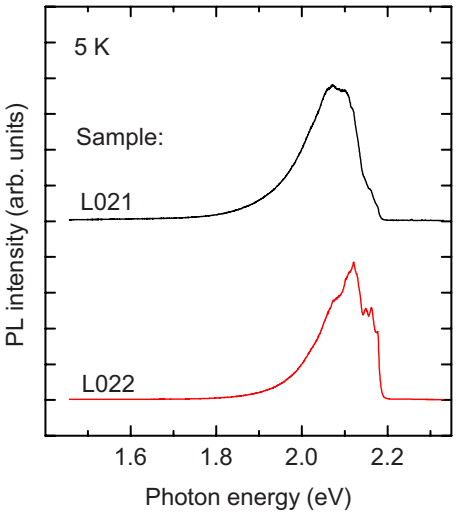


FIG. 1. (Color online) Typical PL spectra measured at 5 K from the GaNP epitaxial layers grown with and without ion collector, denoted by L021 and L022, respectively. The excitation photon energy is 2.33 eV. The spectra are not calibrated by the instrument response.

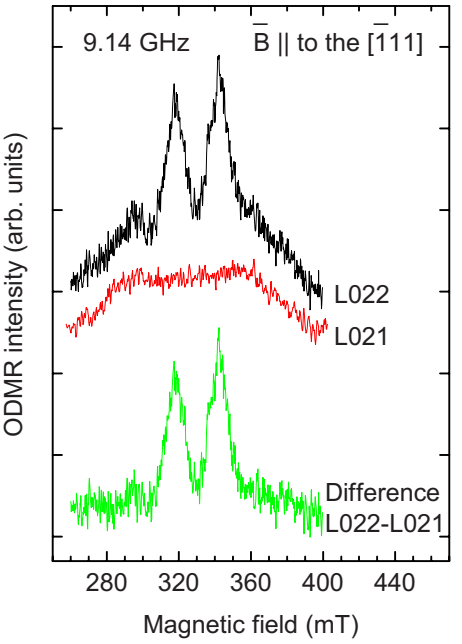


FIG. 2. (Color online) X-band ODMR spectra obtained at 5 K by monitoring the PL from the GaNP epilayers shown in Fig. 1. The magnetic field is parallel to the [$\bar{1}$11] crystallographic direction. The lowest curve displays the difference of the upper two ODMR spectra from the two samples.

application of the ion collector was expected to significantly decrease the number of N ions impinging on the deposited surface. In addition, N flow during the MBE growth was 50% higher for L021 than that for L022 (0.6 and 0.4 sccm, respectively), which is also expected to decrease the ion bombardment during the growth.

Both PL and optically detected magnetic resonance (ODMR) measurements were performed at 5K. The 532 nm line from a solid state laser was employed as a source of photoexcitation above the band-gap energy of the studied GaNP. The resulting PL was dispersed by a 0.5 m single grating monochromator and detected by a charge coupled device camera, in PL experiments. ODMR signals were detected by a Si photodiode as microwave induced changes of PL intensity in the 570–810 nm spectral range by using a combination of optical filters. ODMR experiments were performed at two microwave frequencies, i.e., X-band and Q-band, to minimize uncertainty in interpretation of ODMR data. Typical microwave power employed was 0.2 W, which was amplitude modulated at a frequency of $\simeq 2$ kHz to enable sensitive detection of microwave induced change of PL by a lock-in technique.

## III. EXPERIMENTAL RESULTS

### A. ODMR

Upon above-band-gap optical excitation, both GaNP epilayers exhibit strong PL emissions as shown in Fig. 1. The dominant emission in the visible spectral range peaks at about 2.1 eV, and is known to arise from N-related localized states.[11] ODMR studies of defects in these epilayers were performed by monitoring this PL emission.[12] Figure 2 shows typical ODMR spectra obtained with a magnetic field **B** directed along the [$\bar{1}$11] crystallographic axis of the samples. Both samples show rich-structured ODMR spectra consisting of several overlapping peaks. The ODMR spectrum from the sample L021 is found to be isotropic, within the experimental error. Unfortunately the structure in the ODMR spectrum is not resolved, making identification of the corresponding defect impossible. As it is not the topic of the present study, it will not be discussed further below. On the other hand, ODMR signals from the sample L022 can be decomposed into two parts. The first part is identical to that found in the sample L021. The second component is the stronger lines in the middle-field range of the ODMR spectrum, most clearly seen after subtraction of the first part from the measured ODMR spectrum (see Fig. 2). This new ODMR signal will hereafter be referred to as DD1.

The DD1 ODMR spectrum is dominated by two strong lines, which can originate either from two different defects or from the same defect. In the former case, each defect gives rise to one ODMR line from an unpaired electron of $S=1/2$ at a magnetic field $B=h\nu/\mu_B g$. (Here $h$ is the Planck's constant, $\nu$ is microwave frequency, $\mu_B$ is the Bohr magneton, and $g$ is the $g$ factor of the unpaired electron bound at the defect.) Different $g$ values from the two defects will lead to two ODMR lines separated in field by $\Delta B=(h\nu/\mu_B)[(1/g_1)-(1/g_2)]$ at a given microwave frequency. This line separation should scale linearly with microwave frequency. In the latter case, on the other hand, the two ODMR lines can originate from the same defect as a result of a fine-structure splitting of a spin triplet (effective electron spin $S=1$, nuclear spin $I=0$) or a hyperfine (HF) splitting involving a nuclear spin $I=1/2$ interacting with an unpaired electron spin $S=1/2$. In this case, the ODMR line separation should be independent of microwave frequency, in sharp contrast to the linear dependence expected when two differ-

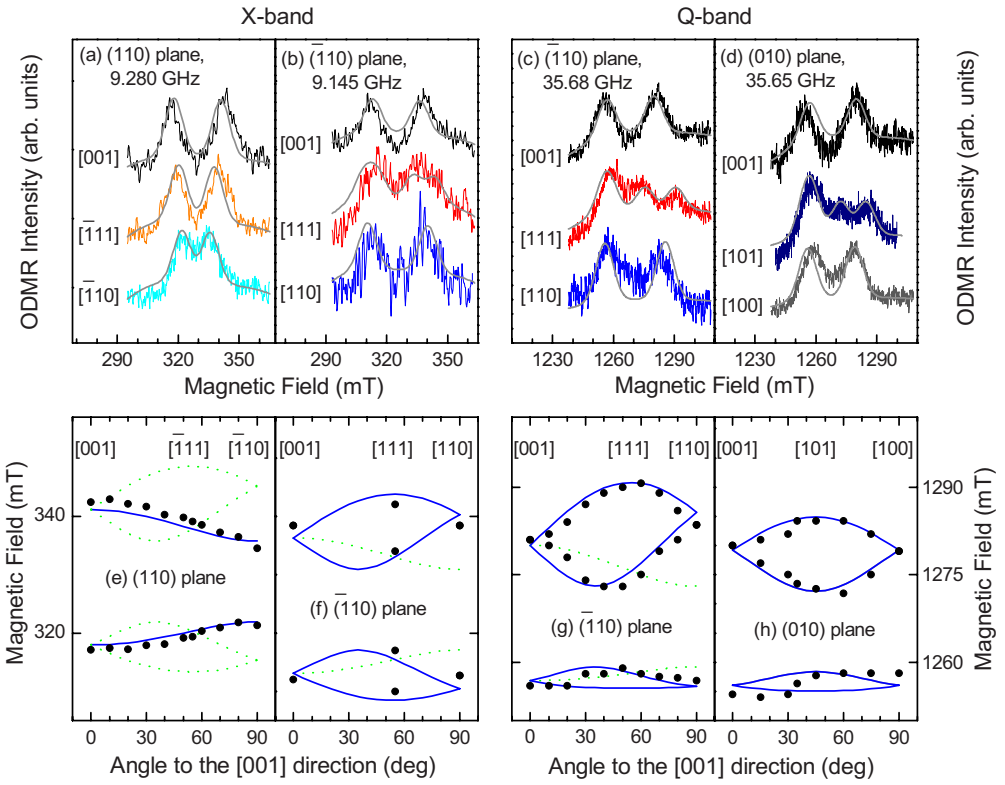


FIG. 3. (Color online) (a)–(d): ODMR spectra at 5 K from the L022 sample when an external magnetic field was rotated in three crystallographic planes: (110), ($\bar{1}$10), and (010), at two different microwave frequencies (i.e., X- and Q-band). The simulated ODMR spectra of the DD1 defect are also displayed, using the spin Hamiltonian parameters given in Table I and assuming a Gaussian line shape and linewidth of 10 mT. A background ODMR signal corresponding to that observed in the L021 sample is also included in the simulated ODMR spectra. (e)–(h): Plots of the peak positions (the full circles) of the ODMR lines from the DD1 defect as a function of the angle between the applied magnetic field and the [001] direction in the (110) and ($\bar{1}$10) and (010) planes. The solid curves correspond to calculated ODMR positions of the DD1 defect using the spin Hamiltonian parameters given in Table I, of which the principal axial axis lies in the ($\bar{1}$10) plane (i.e., two possible ⟨111⟩ orientations). The other two possible defect orientations, of which the axial axis is in the (110) plane, are not experimentally observed (the dashed lines). When the magnetic field was rotated in the (010) plane, see (h), some of the allowed and forbidden defect orientations overlap. In this case, all branches are plotted but only solid lines can be seen.

ent defects are involved (see above). In view of this difference, we carried out ODMR studies at two different microwave frequencies (i.e., X-band and Q-band) in order to determine if one or two defects are responsible for the DD1 ODMR signal. The results are shown in Figs. 3(a)–3(d). It can clearly be seen that the splitting of the ODMR lines when **B** is along the [001] crystal orientation is very similar despite of a change of the microwave frequencies by nearly a factor of four (topmost spectra in Figs. 3(a) and 3(b) vs Figs. 3(c) and 3(d)). This finding leads to a conclusion that the doublet DD1 ODMR signal must originate from the same defect.

To determine if the observed line structure of the DD1 ODMR signal is caused by a fine-structure splitting of a spin triplet or an HF splitting with $I=1/2$, angular dependence of the DD1 ODMR signal was studied in great detail in both microwave frequencies and several crystallographic planes [Fig. 3(a)–3(d)]. In the case of a spin triplet the two ODMR lines are expected to cross each other at some angle, whereas it is not so if the two lines are caused by an HF splitting. Our experimental results seem to favor the latter, see below in Sec. III B for details.

The ODMR spectrum is found to be clearly anisotropic implying a low symmetry of the DD1 defect. The fact that the maximum splitting of the ODMR lines occurs when $\mathbf{B}\|[111]$ indicates that it is likely the principal defect axis. Remarkably, anisotropy of the ODMR signal in the (110) plane [Fig. 3(a)] is very different from that in the crystallographically equivalent ($\bar{1}$10) plane [Fig. 3(b)]. The difference becomes most obvious between $\mathbf{B}\|[110]$ and $\mathbf{B}\|[\bar{1}10]$. The observed difference in the two {110} crystal planes, which are supposed to be equivalent in a zinc-blende crystal lattice of GaNP, is indeed highly surprising. Its implication will be analyzed below with the aid of a spin Hamiltonian and will be further discussed in Sec. IV C.

### B. Spin-Hamiltonian analysis

Analysis of the above intriguing experimental data was performed by a spin Hamiltonian that includes an electron Zeeman term and a central hyperfine interaction term

$$H = \mu_B \mathbf{B} \cdot \mathbf{g} \cdot \mathbf{S} + \mathbf{S} \cdot \mathbf{A} \cdot \mathbf{I}. \quad (1)$$

Here $\mathbf{g}$ is the electronic $g$ tensor and $\mathbf{A}$ is the central hyperfine tensor, in which information about structure and local

TABLE I. Spin-Hamiltonian parameters and the LCAO coefficients of the DD1 complex studied in this work. The axially symmetric axis of the **g** and **A** tensors is along the [111] crystallographic axis.

| | **g** tensor | **A** tensor ($\times 10^{-4}$ cm$^{-1}$) | $\alpha^2$ | $\beta^2$ | $\eta^2$ |
|---|---|---|---|---|---|
| $\parallel$ | 2.002 | 330 | 0.07 | 0.93 | 0.59 |
| $\perp$ | 2.013 | 130 | | | |

environment of the DD1 defect is conveyed. The only reasonable model that can explain all experimental data involves an unpaired electron spin ($S=1/2$) and a nuclear spin $I=1/2$ of the central defect atom, consistent with the qualitative arguments given above in Sec. III A. The anisotropic **g** and **A** tensors are both concluded to have an axial symmetry along a $\langle 111 \rangle$ axis, and their principal values were obtained from a best fit of Eq. (1) to the experimental data [see Figs. 3(e)–3(h) and Table I] using the Easy spin freeware.[13]

Moreover, the experimental results show that only defects oriented along two out of four equivalent $\langle 111 \rangle$ defect orientations are observed in our experiments.[14] The two observed $\langle 111 \rangle$ defect directions cannot be chosen arbitrarily, but are directly determined by the measured angular dependence of the ODMR spectra in Figs. 3(a)–3(d). They are deduced to be in the $(\bar{1}10)$ crystallographic plane, corresponding to the two possible configurations of the interfacial defects residing on the GaNP side of the GaNP/GaP interface (to be discussed in more details below). The simulated ODMR curves are shown in Figs. 3(a)–3(d), using the determined spin Hamiltonian parameters given in Table I and assuming a Gaussian line shape (with a linewidth of 10 mT) for each ODMR transition. The calculated angular dependence of the DD1 ODMR signal is shown in Figs. 3(e)–3(h), using the same set of the spin-Hamiltonian parameters. The solid lines represent the ODMR field positions from the two $\langle 111 \rangle$-oriented DD1 defects that are situated on the GaNP side of the interface and were observed in our experiments. The expected ODMR fields from the other two $\langle 111 \rangle$ orientations on the GaP side of the interface are shown by the dashed lines, which were not observed experimentally. Good agreement between the experimental data and the simulated ODMR results is obtained despite of the simple model, which replicates the salient features of the ODMR spectra reasonably well.

## IV. DISCUSSION

### A. Chemical identification of the defect

The ODMR results in Figs. 3(a)–3(d) imply that the central atom should have 100% natural abundance of $I=\frac{1}{2}$ nuclei. In the MBE-grown GaNP/GaP, where *H* is a common residual contaminant during the growth, phosphorus and hydrogen are the only possible candidates. In order to determine which atom forms the core of the DD1 defect, the L022 sample was annealed for one hour in Ar-ambient at 500 °C. Thermal annealing of GaNP at this temperature is known to effectively remove hydrogen from the crystal.[15] Since annealing did not have any effect on the ODMR signal intensity (not shown here), involvement of hydrogen in the DD1 defect can safely be excluded. A phosphorus atom should thus be at the center of the DD1 defect.

The axial symmetry of the defect, determined from the angular dependence of the ODMR spectra, reveals that it is a complex defect involving a P atom and a partner (or partners) oriented along one out of four permitted $\langle 111 \rangle$ directions. Unfortunately no ligand hyperfine splitting originating from the neighboring partner is resolved in our experiments, prohibiting its chemical identification. The explanation for the absence of ligand hyperfine structure can be twofold. First, the partner has no nuclear spin (i.e., $I=0$) such as a vacancy or an impurity with a vanishing or negligibly small abundance of magnetic isotopes. Second, even when the partner has a nonzero nuclear spin, its nuclear magnetic moment could be too small to lead to experimentally observable hyperfine splitting. We note that the nuclear magnetic moment of the most abundant isotope $^{14}$N (99.63%, $I=1$) of an N atom is more than five times weaker than that of a $^{31}$P atom (100% abundance), which makes N one of possible candidates for the partner in the DD1 defect.

### B. Defect configuration

The P atom involved in the DD1 complex could either reside at a gallium site in the group-III sublattice, giving rise to an antisite $P_{Ga}$, or at one of the three possible self-interstitial sites ($P_i$) in a $T_d$ lattice.[16] From the symmetry point of view, it is not possible to distinguish between the $P_{Ga}$ and the two $T_d$ sites of $P_i$, as they all have the four nearest neighbors along a $\langle 111 \rangle$ axis. An isolated $P_{Ga}$ antisite in its singly positive charge state was previously identified by electron paramagnetic resonance (EPR), characterized by an isotropic and strong HF interaction between the unpaired electron and a $^{31}$P nucleus.[17–20] This interpretation of the early EPR results has been supported by several theoretical studies where an *s*-like deep-level state is expected for an isolated $P_{Ga}^{1+}$ antisite,[20–22] which warrants the observed isotropic and strong HF interaction. In contrast, a *p*-like state was theoretically predicted for a $P_i$ interstitial.[20,21] Following the same line of arguments, many defects with a sizable HF interaction involving a central $^{31}$P atom, commonly occurring in bulk GaP grown by liquid-encapsulated Czochralski, have been interpreted to involve $P_{Ga}$ (and not $P_i$) based on a strong *s*-like character of the wave function and its strong localization at the $^{31}$P atom.[23–30] These assignments have received further support from theoretical prediction that defect formation energy during equilibrium growth greatly favors formation of antisites.[22] To our best knowledge, no defect observed by magnetic resonance in III-phosphides has been attributed to a $P_i$ interstitial defect.

For the studied DD1 defect, we note that the central hyperfine splitting is 3–5 times smaller than the values reported earlier for an isolated $P_{Ga}$ (Refs. 17–19) and defect complexes involving $P_{Ga}$ with $S=1/2$.[23–30] This signifies a significantly reduced overlap of the electron wave function with the P atom at the DD1 defect. This observation could be

explained in terms of (i) strong attraction of electron charge and spin density from $P_{Ga}$ by its partner within the complex defect in the model involving a $P_{Ga}$-related complex, or (ii) a non-*s*-like electron wave function of $P_i$ in the model involving a $P_i$-related complex. In both cases, the wave function of the unpaired electron at the DD1 complex can become anisotropic, leading to the observed anisotropic ODMR spectrum. A detailed analysis of the electron wave function from our ODMR results can be found below in Sec. IV D. Unfortunately it is not possible at present to determine the exact site of the P atom in the DD1 defect, i.e., whether it is an antisite or an interstitial.

### C. Location of the defect

The observation of only two out of four equivalent orientations of the axial defect univocally implies that the DD1 defect is located at the interface between GaP and GaNP, such that structural inversion symmetry of the $T_d$ crystal is broken. The possibility of the DD1 defect being a surface defect, which also has a broken structural inversion symmetry, can be safely ruled out. This is because the GaP capping layers were grown under the same conditions for the L021 and L022 samples and therefore their surfaces are identical, yet the DD1 defect is only present in the L022 sample. If the defect should reside in the bulk of GaNP, on the other hand, all four possible orientations of the ⟨111⟩ axial defect would have been observed with equal ODMR intensity. At the (001) GaNP/GaP interfaces, there are two ⟨111⟩ orientations on either side of the interface that can be the bonding directions to a defect atom situated exactly at the interface plane. We believe that the DD1 defect resides on the GaNP side of the interface for the following reasons. First of all, the defect was introduced in the L022 sample but not in the L021 sample. As the growth conditions were identical for both samples except during the growth of the GaNP layers, this can be taken as strong evidence that the defect was created in GaNP. Parallels can be drawn to the $P_b$ defects at the (111) $Si/SiO_2$ interface. They are interfacial silicon dangling bond defects, in which a silicon atom at the $Si/SiO_2$ semiconductor-insulator interface is back bonded to three other silicon atoms on the Si side but leaves a dangling bond on the $SiO_2$ side due to a missing silicon atom.[1–3] Only the [111] orientation perpendicular to the interface with a dangling bond, i.e., one out of four ⟨111⟩ directions, was detected. An important difference here is that the GaNP/GaP interface lies between two *semiconductor* materials. A tentative and simple model for the DD1 defect complex is depicted in Fig. 4, taking as an example a defect complex involving either a $P_{Ga}$ [Fig. 4(a)] or a $P_i$ [Fig. 4(b)] with a single partner in the nearest-neighbor shell. Due to the presence of a GaP buffer and capping layer, there are two such GaNP/GaP interfaces, i.e., GaNP/GaP buffer layer and GaNP/GaP capping layer. The fact that only two out of the four ⟨111⟩ orientations were observed shows that the DD1 defect is favorably formed only at one of these two interfaces. Based on the discussion on possible mechanisms for the defect formation, to be presented below in Sec. IV E, the DD1 defect will be argued to be more likely formed at the interface between GaNP and the GaP buffer layer than the interface between GaNP and the GaP capping layer.

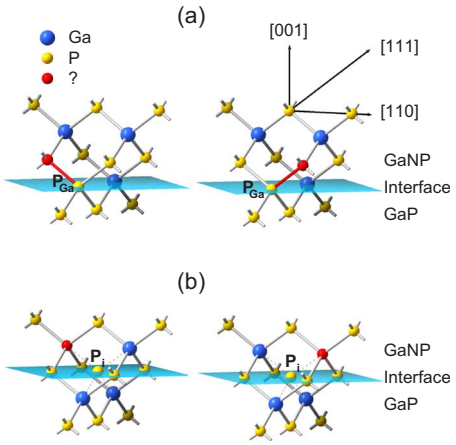


FIG. 4. (Color online) A sketch of tentative models for the DD1 defect complex located at the GaP/GaNP heterointerface. The complex shown here involves (a) a $P_{Ga}$ antisite or (b) a $P_i$ interstitial, bonded to an unknown defect (or defects) in the nearest-neighbor shell (represented by the small dark ball) along a ⟨111⟩ direction on the GaNP side of the interface.

### D. Character of the electron wave function localized at the defect

To get information regarding the degree of localization and the *s* and *p* character of the unpaired electron's wave function at the DD1 defect from the observed hyperfine interactions, we have utilized a one-electron linear-combination-of-atomic-orbitals (LCAO) method.[31] In this method, the wave function for an unpaired electron at the central nucleus can be approximated by a combination of *ns* and *np* valence orbitals

$$\psi = (\alpha\psi_{ns} + \beta\psi_{np}) \times \eta, \tag{2}$$

where $\psi_{ns}$ and $\psi_{np}$ denote *ns* and *np* valence orbitals at the central defect atom, $\alpha^2$ is the fraction of *s*, and $\beta^2$ is the fraction of *p* orbital at the central nucleus, with $\alpha^2+\beta^2=1$. $\eta^2$ is the fraction of the electron wave function at the central nucleus and $n=3$ for the $^{31}P$. Assuming no contribution from the second-order perturbation, components of the axially symmetric $\boldsymbol{A}$ tensor can be described as

$$A_{\parallel} = a + 2b,$$

$$A_{\perp} = a - b, \tag{3}$$

where

$$a = 20\pi\zeta\alpha^2\eta^2|\psi_{3s}(0)|^2 = 197 \pm 20 \times 10^{-4}\ \text{cm}^{-1},$$

$$b = 3\zeta\beta^2\eta^2\langle r_{3p}^{-3}\rangle = 67 \pm 5 \times 10^{-4}\ \text{cm}^{-1}. \tag{4}$$

Here $\zeta = 2gg_N\mu_B\mu_N/15$. $\mu_N$ and $g_N$ denote nuclear magneton and nuclear *g* value, respectively. The unpaired electron density at the nucleus is $|\psi_{3s}(0)|^2$ and the term *a* (i.e., Fermi contact term) provides a direct measure of the 3*s* character of

the wave function since only *s* orbitals have nonzero density at the nucleus. $\langle r_{3p}^{-3} \rangle$ corresponds to the expectation value of $1/r^3$ over the phosphorus $3p$ orbital and $r$ represents the distance between the electron and the nucleus. Parameter $b$ is a measure of the $3p$ character of the unpaired electrons wave function. Using the values derived from the Hartree-Foch-Slater atomic orbitals[32] for the valence $3s$ and $3p$ orbitals of the free $^{31}$P atom ($a=4438\times10^{-4}$ cm$^{-1}$, $b=122\times10^{-4}$ cm$^{-1}$), the parameters $\alpha^2$, $\beta^2$, and $\eta^2$ are estimated and are given in Table I. It is concluded that about $59\pm5\%$ of the wave function is located at the central $^{31}$P atom, much higher than previously reported for $S=\frac{1}{2}$ defects involving $P_{Ga}$ in GaP (ranging from 14 to 23%, as calculated using Eq. (4) based on the reported values of $A$ tensors). In contrary to the $3s$ character previously reported for $P_{Ga}$-related defects[17–20,23–25] (isotropic $\boldsymbol{A}$ tensor), the electron wave function for the DD1 defect is predominantly $3p$-type ($\sim$93%). The observed character of the electron wave function could be attributed to the involvement of either a $P_i$ interstitial complex in the DD1 defect or a $P_{Ga}$ antisite coupled with a defect partner that significantly alters the overall character of the electron state at the DD1 defect.

It should be pointed out that the above analysis by LCAO has not included possible distortion of the electron charge distribution by the electronic potential imposed by the partner of the DD1 complex. Therefore, it could overestimate the contribution of the *p*-like wave function and thereby overestimate the overall degree of electron localization at the defect. In view of the nearly isotropic electron $g$ value, which indicates a rather "pure" spin state with little effect of orbital angular momentum, this scenario seems to be very likely here.

### E. Defect formation

The fact that the DD1 defect was only observed in the L022 sample, which was grown under the conditions with more severe bombardment of N ions, strongly indicates that the defect formation is facilitated by ion damage. There are two possible mechanisms for the defect formation that are promoted by ion bombardment.

(1) In the first mechanism, the DD1 defect was directly generated at the interface between GaNP and the GaP buffer layer due to irradiation of N ions on the surface of the GaP buffer layer during and immediately after growth interruption. The growth interruption was applied prior to the growth of GaNP, when the shutter of the Ga cell was closed and the RF plasma was started and stabilized. Though the shutter of the RF-plasma cell was closed during the interruption, it was still possible that leaking N ions could arrive at the surface of the GaP buffer layer. More severely, immediately after the growth interruption, the shutter of the RF-plasma cell opened and the growing surface was directly exposed to N-ion bombardment. When the growth of the GaP capping layer started, on the other hand, the RF plasma was turned off and thus formation of the DD1 defect was less likely at the interface between GaNP and the GaP capping layer.

(2) In the second mechanism, intrinsic defects such as $P_{Ga}$ antisites, $P_i$ self-interstitials and vacancies were created in the GaNP epilayer. During the growth, these defects could migrate until energetically most favorable sites had been found, e.g., near other defects or at the interfaces, forming thermally stable defects. Although the specific process of defect migration leading to the formation of the DD1 defect complex cannot be deduced from the present study, it is clear that the growth conditions favored the formation of the DD1 defect (i.e., a P-related defect complex) at the GaNP/GaP interface. The preferential formation of the defect at the interface could be caused by the difference in formation energy of the defect between bulk and interface, and between GaNP and GaP side of the interface, under the influence of an electric field (caused by the electronic band offset and charge transfer) and/or strain field (caused by the lattice mismatch) near the heterointerface. It should be noted that the DD1 defect complex is indeed very stable, confirmed by our post-growth thermal annealing experiments at 500 °C. No effect on the ODMR intensity of the DD1 defect was observed after annealing.

We should note that, in Ga(In,Al)NP with higher N compositions, $Ga_i$ interstitial related defects and an unknown defect with a $g$ value around 2 are dominating in ODMR spectra[33,34] and the DD1 has not been observed. A possible explanation is that the much stronger ODMR signals from the $Ga_i$ defects and the unknown $g=2$ defect have completely obscured the ODMR signal from the DD1 defect, even the latter is present.

## V. SUMMARY

Our ODMR studies of GaNP have revealed the presence of a paramagnetic defect, exhibiting a hyperfine interaction between an unpaired electronic spin ($S=1/2$) and a central nuclear spin $I=\frac{1}{2}$ of $^{31}$P. The defect is concluded to be a complex involving a $P_{Ga}$ antisite or a $P_i$ interstitial with a neighboring partner aligned along a $\langle 111 \rangle$ direction, from detailed angular dependence studies of the ODMR spectra at both X- and Q-band microwave frequencies. The principal $g$ and $A$ values, $g_\perp=2.013$, $g_\parallel=2.002$, $A_\perp=130\times10^{-4}$ cm$^{-1}$, and $A_\parallel=330\times10^{-4}$ cm$^{-1}$, are obtained from a spin Hamiltonian analysis. The interface nature of the defect is clearly evident from the absence of the ODMR lines originating from two out of four equivalent $\langle 111 \rangle$ orientations. A simple LCAO analysis suggests that the electron wave function at the defect is predominantly $p$ type at the P atom (93%), with 7% admixture of $s$ type. The fraction of the $p$-like state was found to be markedly higher than that previously reported for $P_{Ga}$-complexes in GaP, which could at least partly be contributed by a strong distortion of the charge and spin density around the P atom due to the presence of the partner in the DD1 complex. The defect formation is shown to be triggered by severe nitrogen ion bombardment under nonequilibrium growth conditions during solid-source molecular beam epitaxy.

**ACKNOWLEDGMENTS**

Financial support by the Swedish Research Council (VR), the Swedish Energy Agency, and the Wenner-Gren Foundations is greatly appreciated. The authors would also like to express their gratitude to Carina Höglund for aligning the samples with the aid of x-ray diffraction.

[1] For a review of electron spin resonance in MOS systems, see P. M. Lenahan and J. F. Conley, Jr., J. Vac. Sci. Technol. B **16**, 2134 (1998).

[2] Y. Nishi, K. Tanaka, and A. Ohwada, Jpn. J. Appl. Phys. **11**, 85 (1972).

[3] P. J. Caplan, E. E. Poindexter, B. E. Deal, and R. R. Razouk, J. Appl. Phys. **50**, 5847 (1979).

[4] P. Krispin, Mater. Sci. Eng., B **28**, 387 (1994).

[5] E. P. Valcheva, Appl. Phys. A: Mater. Sci. Process. **65**, 39 (1997).

[6] For a review, see *Physics and Applications of Dilute Nitrides*, edited by I. A. Buyanova and W. M. Chen (Taylor & Francis, New York, 2004).

[7] For a review, see *Dilute III–V Nitride Semiconductors and Material Systems*, Springer Series in Material Science, edited by A. Erol (Springer, Berlin, 2008), Vol. 105.

[8] H. Yonezu, Semicond. Sci. Technol. **17**, 762 (2002).

[9] K. Momose, H. Yonezu, Y. Fujimoto, Y. Furukawa, Y. Motomura, and K. Aiki, Appl. Phys. Lett. **79**, 4151 (2001).

[10] R. J. Welty, Y. G. Hong, H. P. Xin, K. Mochizuki, C. W. Tu, and P. M. Asbeck, in *Proceedings of the 2000 IEEE/Cornell Conference on High Performance Devices*, edited by M. G. Alderstein (IEEE, Piscataway, NJ, 2000), pp. 33–40.

[11] I. A. Buyanova, G. Yu. Rudko, and W. M. Chen, Appl. Phys. Lett. **80**, 1740 (2002).

[12] For a review on ODMR, see W. M. Chen, Thin Solid Films **364**, 45 (2000).

[13] S. Stoll and A. Schweiger, J. Magn. Reson. **178**, 42 (2006).

[14] If present, ODMR intensities from the defect with the other two orientations must be more than four times weaker than that of the dominant ones judging from the experimental signal-to-noise ratio. Otherwise, they would have been detected.

[15] A. Polimeni, M. Bissiri, M. Felici, M. Capizzi, I. A. Buyanova, W. M. Chen, H. P. Xin, and C. W. Tu, Phys. Rev. B **67**, 201303(R) (2003).

[16] In principle, there could be a third possibility for the origin of the P atom at the core of the DD1 defect. It could be a P lattice atom but having a broken bond along one of the four ⟨111⟩ bonding directions when one of its neighboring Ga atoms was replaced by a defect/impurity. Lattice distortion of either the P atom or this neighboring defect/impurity atom, or both, is required in this case in order to explain the observed trigonal symmetry for the DD1 defect. The problem with this model is that this defect/impurity partner on the Ga site shares four (or two sets of two at the interface) identical P lattice atoms as the nearest neighbors, if there is no N atom involved here. It is not clear why it should then only favor one with a broken bond, forming a defect with a trigonal symmetry. It is interesting to note that, if the defect partner is a missing Ga atom, the DD1 defect should in fact be equivalent to a Ga vacancy in GaP. The latter was previously shown to maintain high symmetry with HF interaction involving all four nearest-neighbor P atoms [T. A. Kennedy, N. D. Wilsey, J. J. Krebs, and G. H. Stauss, Phys. Rev. Lett. **50**, 1281 (1983)]. It is not clear if the presence of N atoms and the interface could provide a mechanism for the formation of the observed defect. Nevertheless, in view of the difficulties mentioned above, this model seems to be less plausible than the models involving a $P_{Ga}$ antisite or a $P_i$ interstitial.

[17] U. Kaufmann, J. Schneider, and A. Räuber, Appl. Phys. Lett. **29**, 312 (1976).

[18] K. P. O'Donnell, K. M. Lee, and G. D. Watkins, Solid State Commun. **44**, 1015 (1982).

[19] J. J. Lappe, B. K. Meyer, and J.-M. Spaeth, Inst. Phys. Conf. Ser. **95**, 249 (1989).

[20] M. Jaros, J. Phys. C **11**, L213 (1978).

[21] S. Goettig and C. G. Morgan-Pond, Phys. Rev. B **42**, 11743 (1990).

[22] See A. Höglund, C. W. M. Castleton, and S. Mirbt, Phys. Rev. B **72**, 195213 (2005), and references therein.

[23] B. K. Meyer, Th. Hangleiter, J.-M. Spaeth, G. Strauch, Th. Zell, A. Winnacker, and R. H. Bartram, J. Phys. C **18**, 1503 (1985).

[24] U. Kaufmann and J. Schneider, Adv. Electron. Electron Phys. **58**, 81 (1982).

[25] T. A. Kennedy and N. D. Wilsey, Inst. Phys. Conf. Ser. **46**, 375 (1979).

[26] N. Killoran, B. C. Cavenett, M. Godlewski, T. A. Kennedy, and N. D. Wilsey, J. Phys. C **15**, L723 (1982).

[27] W. M. Chen, H. P. Gislason, and B. Monemar, Phys. Rev. B **36**, 5058 (1987).

[28] W. M. Chen, B. Monemar, and M. Godlewski, Phys. Rev. B **37**, 2564 (1988).

[29] H. J. Sun, C. F. Rong, and G. D. Watkins, Phys. Rev. B **50**, 10619 (1994).

[30] M. Godlewski, W. M. Chen, and B. Monemar, Defect Diffus. Forum **62-63**, 107 (1989).

[31] G. D. Watkins and J. W. Corbett, Phys. Rev. **121**, 1001 (1961).

[32] J. R. Morton and K. F. Preston, J. Magn. Reson. **30**, 577 (1978).

[33] N. Q. Thinh, I. P. Vorona, I. A. Buyanova, W. M. Chen, L. Sukit, S. B. Zhang, Y. G. Hong, C. W. Tu, A. Utsumi, Y. Furukawa, S. Moon, A. Wakahara, and H. Yonezu, Phys. Rev. B **70**, 121201 (2004).

[34] D. Dagnelund, I. A. Buyanova, T. Mchedlidze, W. M. Chen, A. Utsumi, Y. Furukawa, S. Moon, A. Wakahara, and H. Yonezu, Appl. Phys. Lett. **88**, 101904 (2006).